Supporting Information

Maskarinec et al. 10.1073/pnas.0904565106

SI Text

Characterization of FN-Modified Films. Comparison of the relative amounts of covalently attached FN on polyacrylamide (PA) samples made with varying percentages of cross-linker was conducted using a commercially available bicinchoninic acid (BCA) assay kit (Sigma–Aldrich). The relative protein concentration is quantified by measuring the absorbance at 562 nm using a plate reader and comparing the measured values to a standard curve generated using known amounts of FN (Sapphire, Tecan Group Ltd.). A set of FN-modified samples (lacking embedded microspheres) was prepared as described above and placed in a six-well plate (Becton Dickinson). Negative controls consisting of unmodified samples made with similar cross-linker percentages (% BIS) were also prepared. All samples were then treated for 1 h at 60 °C followed by an absorbance reading. These experiments were repeated three times in triplicate for each % BIS.

The fibronectin surface density for samples made with varying % BIS were found to be similar (0.189 ± 0.108 μg/mm^2 for 0.015% BIS, and 0.171 ± 0.101 μg/mm^2 for 0.0075% BIS) and lie within the standard deviation calculated from the tested samples. These results confirm that the prepared samples display similar amounts of FN on the surface, and that changes in cell behavior result from differences in mechanical properties and not to some difference in the chemical composition of the surfaces.

Sample Characterization. The thickness of the sample was determined by calculating the distance from the bottom of the glass surface to the disappearance of bead fluorescence at the top of the sample using a confocal microscope. The sample thicknesses were controlled by adjusting the total volume of the acrylamide mixture used to make the samples.

The mechanical properties of the substrates were determined by performing both unconfined and confined compression testing on cylindrical polyacrylamide specimens using a custom-built compression setup (1) (Fig. S1). The typical sample dimensions were 8 mm in diameter and 4 mm in height. The displacements during each compression increment were controlled using a digital micrometer with a resolution of 1 μm. The resulting nominal force was measured using a 10 g load cell (A.L. Design). For each volume fraction of BIS cross-linker used, 6–8 samples were tested in both confined and unconfined uniaxial compression.

For unconfined tests, gel samples were cast in a circular washer secured to the bottom of a 60-mm diameter plastic Petri dish. After polymerization (≈2–5 min), the washer was removed from the dish and the sample was hydrated and left covered at room temperature overnight to ensure adequate swelling. Before compression, the alignment of the setup with the sample was inspected to ensure pure compression along the nominal loading axis. The samples were compressed between the top platen of the compression setup and the bottom of the Petri dish with a nominal strain increment of 1–2%. Nominal strain increments are defined by the ratio of the displacement increment resulting from the compression to the original sample height. Force values were obtained continuously during each 5-min increment to detect any time-dependent relaxation of the material during the compression. The total applied nominal compressive strain was approximately 13–15%. After complete loading, the sample was successively unloaded using the same strain increments to record the entire loading-unloading cycle.

To determine Poisson's ratio for each polyacrylamide gel, cylindrical specimens were cast and polymerized in a confined Teflon sleeve 15 mm in diameter and approximately 8 mm in height. Samples were hydrated following the same protocol as described above. The samples were compressed following the same loading-unloading protocol as for the unconfined test.

Mechanical Characterization Using Confined and Unconfined Compression Testing. The mechanical properties of polyacrylamide specimens were determined by performing both unconfined and confined compression using a custom-built compression setup (1) (Fig. S1). Fig. S2 shows the raw data for an incremental loading cycle highlighting negligible time-dependent material behavior, and Fig. S3 shows the loading-unloading stress strain curve for a typical sample following unconfined compression. The Young's modulus for the polyacrylamide samples was calculated from each stress-strain curve using the relationship:

$$E = \frac{\sigma}{\varepsilon} = \frac{\frac{F}{A}}{\frac{\Delta h}{h}},$$

where σ and ε denote the uniaxial stress and strain, and can be expressed as the applied force per sample contact area, and change in sample height over its original height.

Table S1 summarizes the unconfined compression test results for two different cross-linker volume fractions.

Using the determined Young's modulus value of the unconfined test case and observing that further compression beyond an initial compression strain of approximately 0.25% was not possible (due to the Poisson effect) during confined compression tests, Poisson's ratio was determined to be approximately 0.48–0.5 according to the following equation:

$$\bar{E} = \frac{\sigma}{\varepsilon} = \frac{1-\nu}{(1+\nu)(1-2\nu)}E,$$

where E denotes the measured confined compression modulus, ν is the Poisson's ratio, and E is the Young's modulus as determined from unconfined compression test. From this set of experiments, Poisson's ratio was taken to be 0.5, and the material behavior is described as a linearly elastic, isotropic, and incompressible for all traction force calculations.

In addition, dynamic mechanical shear (DMA) measurements measuring the loss and storage modulus of the polyacrylamide substrata were performed. The results from the DMA measurements showed both moduli, G′ (storage) and G″ (loss), to be time-independent over a frequency range from 0.01–100 rad/s, and the ratio $G''/G' \ll 1$, which is consistent with the mechanical characterization results from the uniaxial compression experiments.

Comparison of Surface Displacements and Traction Forces for Different Substrate Moduli. Fig. S4 shows contour surface plots of measured displacements and calculated traction forces for polyacrylamide substrates of different Young's moduli. The two upper plots show contours of the magnitude of the 3-D displacement vector with the in-plane vector components shown as white arrows. The left and right bottom plots show contour plots of the magnitude of the 3-D surface traction force vector with the in-plane traction forces shown as white arrows. The figure shows

that cell traction forces scale approximately linearly with material's Young modulus as had been observed in ref. 2. The displacements and traction forces in the left column were calculated on a polyacrylamide gel with a Young's modulus of 0.82 kPa, whereas the displacements and traction force data in the right column corresponds to a Young's modulus of 9.64 kPa.

Traction Force Inhibition Using Blebbistatin. Time-lapse imaging of fibroblasts was performed before and after treatment with blebbistatin to demonstrate that measured displacements were the result of cell-generated forces and not the result of thermal fluctuations within the substrate (Fig. S5). Blebbistatin is commonly used in traction force measurements to inhibit actinomyosin contraction in nonmuscle cells (3, 4). Fig. S5*B* shows the average maximum displacements achieved by a single cell at time points before and after treatment with blebbistatin. After blebbistatin administration (injected at stack 3), there is a notable decrease in the average maximum displacement. Despite the cell's presence, there are no detectable displacements after 35 min. Identical experiments performed without cells and in the presence of blebbistatin yielded no notable displacements, establishing that all measured displacements are cell-induced.

Global Force and Moment Balance. The net forces and moments on several control volumes including the entire volume image stack were computed at every time increment and static equilibria were found to be satisfied. This means that for any control volume within the imaged volume stack the summation of traction forces and moments summed up to the order of approximately 10^{-3} to 10^{-4} mN and approximately 10^{-5} to 10^{-4} mN·mm, for forces and moments respectively. This is on the same order of magnitude as the summation of forces for the control case control volumes where no cells and no external forces where present (control samples). Hence, these numbers represent the baseline noise of the DVC-LSCM technique and are consistent with the stated displacement sensitivity of 0.12 μm.

1. Franck C, Hong S, Maskarinec SA, Tirrell DA, Ravichandran G (2007) Three-dimensional full-field measurements of large deformations in soft materials using confocal microscopy and digital volume correlation. *Exp Mech* 47:427–438.
2. Balaban NQ, et al. (2001) Force and focal adhesion assembly: A close relationship studied using elastic micropatterned substrates. *Nat Cell Biol* 3:466–472.
3. Beningo KA, Hamao K, Dembo M, Wang YL, Hosoya H (2006) Traction forces of fibroblasts are regulated by the Rho-dependent kinase but not by the myosin light chain kinase. *Arch Biochem Biophys* 456:224–231.
4. Bhadriraju K, et al. (2007) Activation of ROCK by RhoA is regulated by cell adhesion, shape, and cytoskeletal tension. *Exp Cell Res* 313:3616–3623.

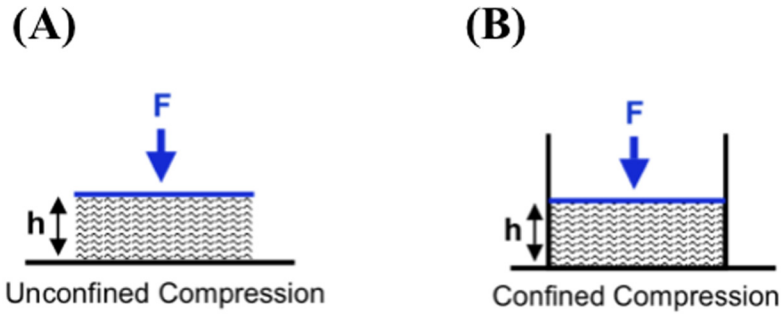

Fig. S1. Detailed schematic of the compression tests. Unconfined compression tests (*A*), confined compression tests (*B*).

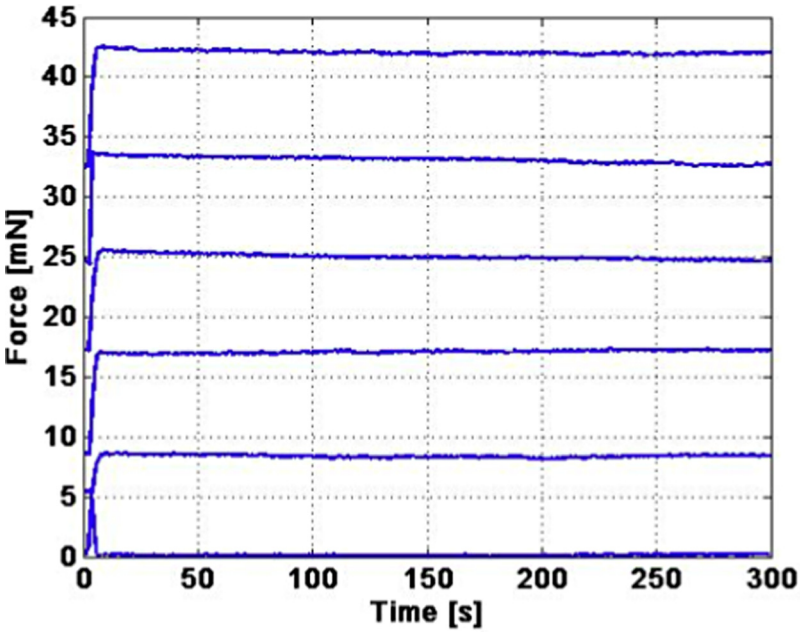

Fig. S2. Incremental loading tests using polyacrylamide samples highlighting the negligible time-dependent relaxation behavior of the material. Force values were obtained continuously during 5 min-increments.

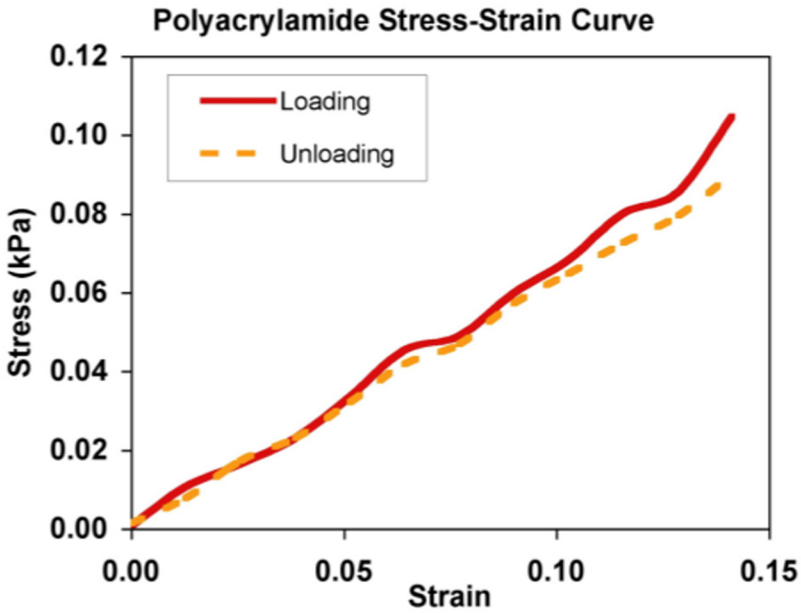

Fig. S3. Representative stress-strain curves of loading and unloading cycles on cylindrical hydrated polyacrylamide samples demonstrating a linear elastic material response with negligible hysteresis.

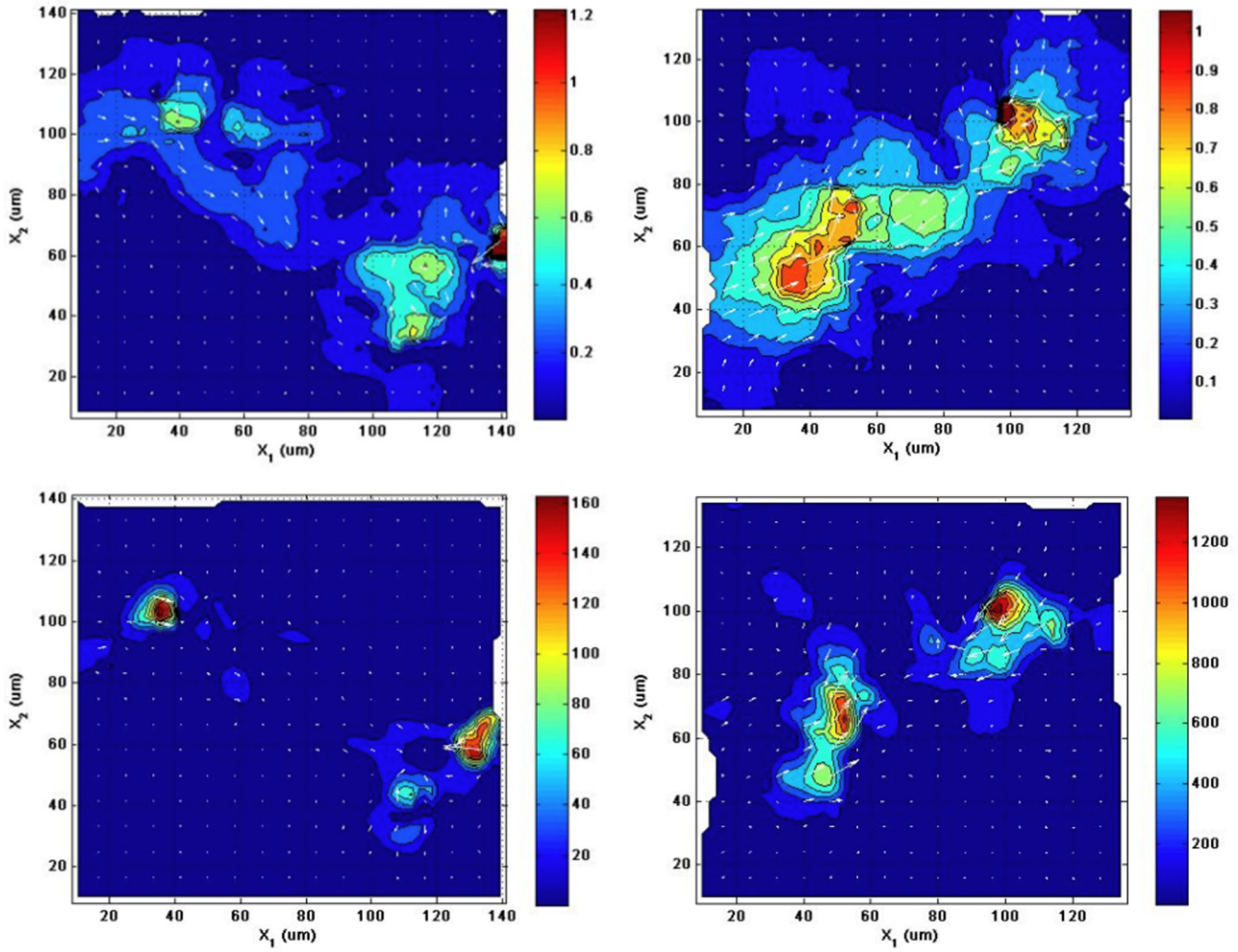

Fig. S4. Comparison of displacements and traction forces contour surface plots for soft substrates (*Left*, E = 0.82 kPa) and stiff substrates (*Right*, E = 9.64 kPa), respectively. Displacements are shown in micrometers (color bar in *Top* two plots); traction forces are shown in pN/μm^2 (color bar *Bottom* two plots).

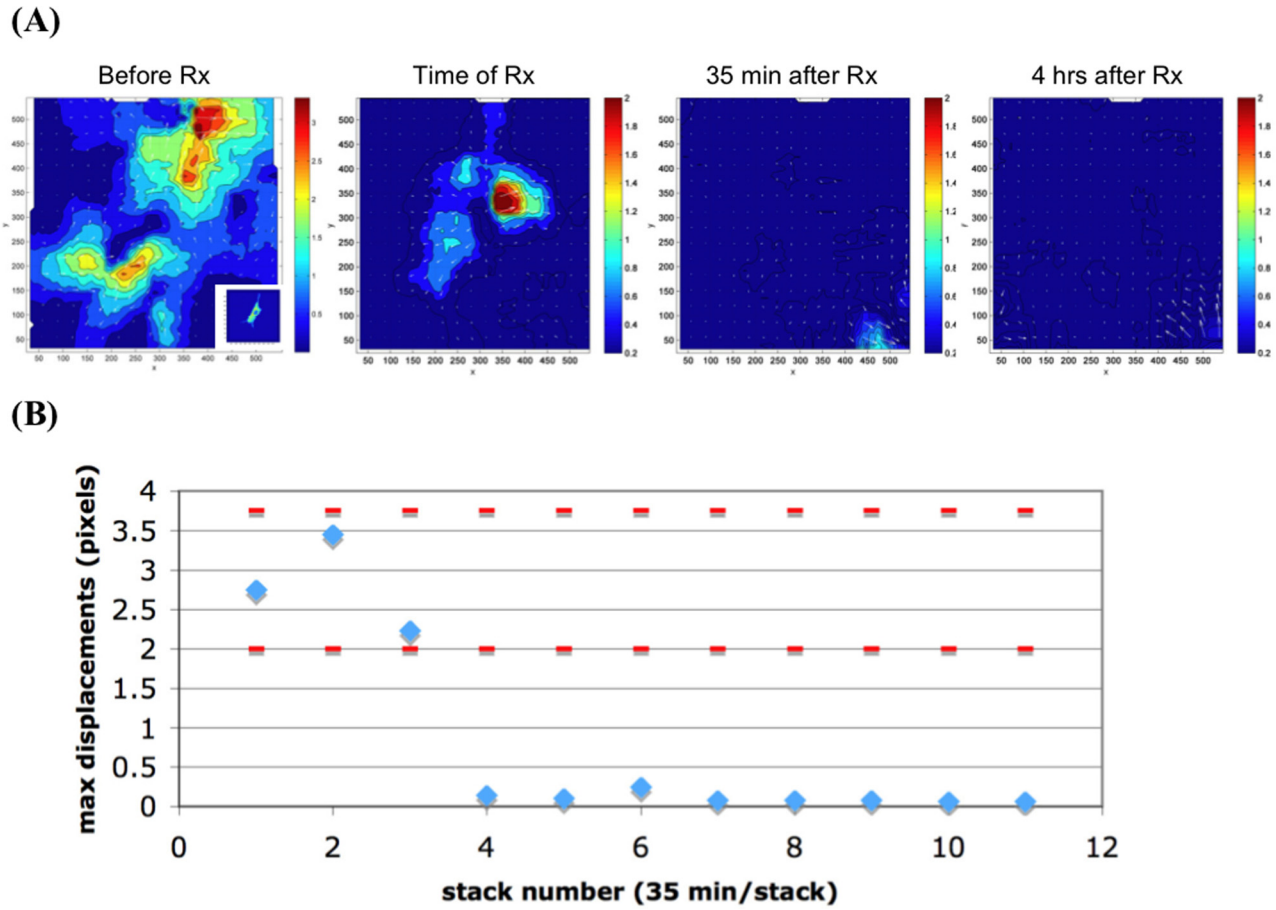

Fig. S5. Traction force inhibition using blebbistatin. Superimposed planar images of cells and displacement contours before and after treatment (Rx) with blebbistatin (*A*), plot of average maximum displacements measured before and after blebbistatin treatment (*B*). Confocal stacks were obtained every 35 min.

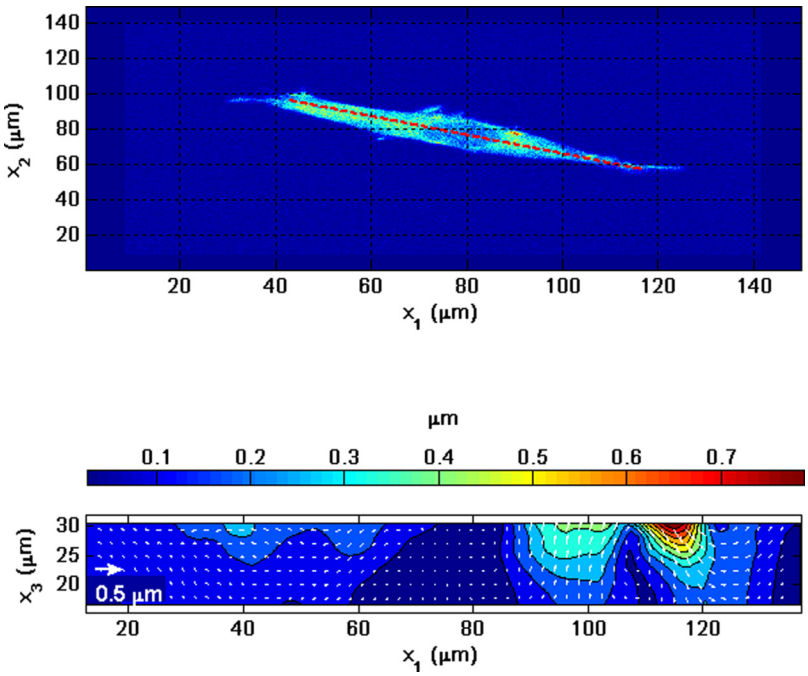

Movie S1. Time-lapse video of cell movement visualized by confocal microscopy of cellular GFP-actin (*Top*) and the corresponding three-dimensional cell-induced displacement field (*Bottom*) under the long axis of the cell highlighted by the red line (*Top*). Confocal images were obtained every 35 min. The color bar represents the magnitude of the total 3-D displacement vectors, and the arrows represent the displacement vectors in the x-z ($x_1 - x_3$) plane.

Movie S1 (AVI)

Table S1. Mechanical characterization results for polyacrylamide substrates

Cross-linker volume fraction	Young's modulus (kPa)
0.015% BIS	9.64 ± 1.12
0.0075% BIS	0.82 ± 0.23